Neuro-Oncology
27(4), 916–931, 2025 | https://doi.org/10.1093/neuonc/noae278 | Advance Access date 4 January 2025

Genome-wide CRISPR-Cas9 screens identify BCL family members as modulators of response to regorafenib in experimental glioma

Lara Annina Haeusser, Hannes Becker, Laurence Kuhlburger, Marcello Zago, Bianca Walter, Foteini Tsiami, Sarah Erdmann, Jil Trampert, Surender Surender, Aaron Stahl, Markus Templin, Eileen Wegner, Tobias Schmidt, Christian Schmees, Nicolas Casadei, Lisa Sevenich, Manfred Claassen, Sven Nahnsen, Susanne Beck, Daniel Josef Merk, and Ghazaleh Tabatabai

All author affiliations are listed at the end of the article

Corresponding Author: Ghazaleh Tabatabai, Prof. Dr. med. Dr. rer. nat., Department of Neurology and Interdisciplinary Neuro-Oncology, Hertie Institute for Clinical Brain Research, University Hospital Tübingen, Eberhard Karls University Tübingen, Hoppe-Seyler-Strasse 3, 72076 Tübingen, Germany (ghazaleh.tabatabai@uni-tuebingen.de)

Abstract

Background. Registered systemic treatment options for glioblastoma patients are limited. The phase II REGOMA trial suggested an improvement of median overall survival in progressive glioblastoma by the multi-tyrosine kinase inhibitor regorafenib. This has not been confirmed by GBM AGILE. So far, regorafenib has been administered as monotherapy or as an addition to standard of care in newly diagnosed glioblastoma. Rational combination therapies involving regorafenib might be a reasonable strategy. Here, we aimed at identifying functionally instructed combination therapies involving regorafenib.

Methods. We applied a genome-wide CRISPR-Cas9-based functional genomics target discovery approach using activation and knockout screens followed by genetic, pharmacological, functional validations. Regorafenib-induced molecular alterations were assessed by RNA sequencing and DigiWest. We investigated selected functionally instructed combination therapies in three orthotopic glioma mouse models in vivo (syngeneic SMA560/VM/Dk model and two xenograft models) and performed immunohistochemistry of post-treatment brains.

Results. We identified potential modifiers of regorafenib response, including *BCL2*, *BCL2L1*, *ITGB3*, *FOXC1*, *SERAC1*, *ARAF*, and *PLCE1*. The combination of regorafenib with Bcl-2/Bcl-x_L inhibition was superior to both monotherapies alone in vitro, ex vivo, and in vivo. We identified regorafenib-induced regulations of the Bcl-2 downstream target chemokine receptor 1 (CCR1) as one potential underlying molecular mediator. Furthermore, regorafenib led to changes in the myeloid compartment of the glioma-associated microenvironment.

Conclusions. This preclinical study uses a functional genomics-based target discovery approach with subsequent validations involving regorafenib. It serves as a biological rationale for clinical translation. Particularly, an investigation of the combination of regorafenib plus navitoclax within a clinical trial is warranted.

Key Points

- Functional genomics identify modifiers of response to regorafenib
- Regorafenib-induced CCR1 inhibition contributes to a synergistic efficacy of regorafenib plus navitoclax
- Regorafenib modulates the myeloid compartment

Importance of the Study

This study used a genome-wide CRISPR-Cas9-based functional genomics approach to discover and validate targets modifying the therapeutic efficacy of regorafenib in experimental glioma. This experimental strategy led to the identification of targets for novel combination therapies in glioma, which significantly enhanced the efficacy of regorafenib treatment in vitro, ex vivo, and in vivo. From a translational perspective, the combination of regorafenib with B-cell lymphoma (Bcl-)2/Bcl-x_L inhibition using navitoclax is a promising and feasible strategy for immediate clinical translation. On a molecular level, regorafenib-mediated inhibition of the Bcl-2 target C-C motif chemokine receptor 1 (CCR1) was identified as a potential mediator of synergistic effects of regorafenib and navitoclax. In line with this, the intratumoral myeloid compartment was modified by regorafenib in the syngeneic SMA560/VM/Dk mouse model in vivo. Taken together, this study contributes a preclinical biological rationale for combination therapies involving regorafenib and can inform the design of clinical trials.

Glioblastoma are incurable primary tumors of the central nervous system.[1] Even in selected clinical trial populations, median overall survival of glioblastoma patients is about 1.5 years. Available treatment modalities include maximal safe neurosurgical resection, radiation therapy, alkylating chemotherapy and tumor treating fields.[2–4]

Genetic alterations of receptor tyrosine kinases (RTKs) are common in glioblastoma, often leading to a constitutive activation of tumor-promoting pathways. Targeting of RTKs is thus in principle a promising treatment strategy.[5,6] Furthermore, glioblastoma is a highly vascularized tumor calling for antiangiogenic strategies, particularly involving the vascular endothelial growth factor (VEGF) and VEGFR axis. Clinical trials investigating bevacizumab or sorafenib in glioblastoma did not improve overall survival, however, and small molecular inhibitors cediranib and sunitinib also failed in this regard.[5–9]

Regorafenib inhibits several RTKs including VEGFR 1-3, angiopoietin-1 receptor (TIE2), tyrosine kinase KIT, rearranged during transfection (RET), rapidly accelerated fibrosarcoma (RAF)-1, v-raf murine sarcoma viral oncogene homolog B1 (BRAF), platelet-derived growth factor receptor (PDGFR), and fibroblast growth factor receptor.[10–12] Regorafenib revealed preferential potency in the inhibition of PDGFR, VEGFR-2, TIE2 compared with other multi-tyrosine kinase inhibitors[12–16] and is a type 2 kinase inhibitor which binds to inactive kinases in an ATP-independent way.[17] It is registered for advanced hepatocellular carcinoma, metastatic colorectal cancer, and gastrointestinal stromal tumors,[18–20] is an oral compound and has manageable side effects.[21,22]

The phase II REGOMA trial in progressive glioblastoma revealed a median overall survival of 7.4 months (regorafenib) compared to 5.6 months (lomustine),[21] and observational studies confirmed these results.[23–25] The regorafenib arm in the Glioblastoma Adaptive Global Innovative Learning Environment (GBM Agile) platform trial did not show a significant improvement of survival (probability of 0.24) and was terminated with a mean hazard ratio for overall survival of 1.12 in 126 patients in the progressive disease arm.[26] A post hoc translational investigation of the REGOMA study group revealed that a molecular signature comprising *HIF1A*, *CDKN1A*, miR-3607-3p, miR-301a-3p, miR-93-5p enabled the identification of a patient subgroup with prolonged survival after regorafenib. Additionally, an association between thyroid function and response to regorafenib in glioblastoma has been suggested. Both findings will need further validation.[27,28] Regorafenib has been mainly used as a single agent (in progressive disease) or as an addition to standard of care (in newly diagnosed glioblastoma).[29] A parallel cohort phase 2 study of regorafenib plus nivolumab did not support further evaluation of this combination (NCT04704154).[30] Further biological rationales are warranted to inform the design of combination therapies.

Our scientific aim was to address this research gap by an innovative target discovery and validation approach using genome-wide CRISPR-Cas9 activation and knockout screens followed by investigations of functionally instructed combination therapies.

Methods

CRISPR-Cas9 Genome-Wide Activation Screens

We used dCas9-VP64 cell lines for transduction with the Calabrese P65-HSF library (Set A) for genome-wide gene activation.[31] This library consists of 56,762 sgRNAs targeting 18,885 gene promotors. We transduced dCas9-VP64 expressing cells with a predetermined volume of lentiviral-packaged Calabrese library to attain a maximum of 30% transduction efficiency, while ensuring a 500× library coverage. We conducted transductions in technical duplicates. 24 h posttransduction, we used a predetermined puromycin concentration for five days to select transduced cells. In parallel, we assessed transduction efficacy through an in-line assay. On day 7 of the screen, we split 30×10^6 cells for each duplicate into drug or corresponding DMSO arms, maintaining a 500× coverage. Throughout the 14-day screen period, we passaged all surviving cells from screens under continuous drug treatment. In DMSO control arms, a minimum library coverage of 500× was maintained at all steps. After 14 days of drug treatment, we collected 50×10^6 cells from DMSO control arms and all remaining cells for treatment conditions for storage at –80 °C and subsequent DNA extraction.

CRISPR-Cas9 Genome-Wide Knockout Screens

For genome-wide CRISPR-Cas9 knockout screens, we used the Brunello library with 76,441 sgRNAs targeting 19,114 genes.[32] We transduced Cas9-expressing cell lines with a predetermined volume of lentiviral-packaged Brunello library to attain a maximum 30% transduction efficiency, ensuring a 500× library coverage. We conducted transductions in technical duplicates. 24 h posttransduction, we used a predetermined puromycin concentration for 5 days to select transduced cells. In parallel, we assessed transduction efficacy through an in-line assay. On day 7 of the screen, we split 40×10^6 cells for each duplicate into drug or corresponding DMSO arms, thus maintaining a 500× coverage. Throughout the 14-day screen period, we passaged all arms under ongoing drug or vehicle treatment with maintaining a minimum library coverage of 500×. After 14 days, we collected 60×10^6 cells of each condition for storage at –80 °C for subsequent DNA extraction.

CRISPR-Cas9 Screen Analysis

We extracted genomic DNA from frozen screen cell pellets using the QIAmp DNA Blood Kit (Qiagen, Venlo, NL) according to manufacturer's instructions. DNA equivalent to a cell number representing 500× library coverage was sent to the Broad Institute of MIT and Harvard for next-generation sequencing following a previously described protocol.[32] Sequencing data from corresponding plasmid pools of Brunello and Calabrese libraries used to generate lentiviral particles used in this study were provided by the Broad Institute. Quality control assessments of raw sequencing data were done using FastQC (v0.11.9). Reads were mapped to corresponding sgRNA libraries and counted using PoolQ (3.4.3). PoolQ processed in average a total of 42 million reads in all Brunello samples and 28.4 million in all Calabrese DMSO-treated samples, with an average mapping rate of 88.5% and 87.1%. Each sgRNA instance was counted and a tab delimited count file was generated. We used a custom script (available at https://github.com/qbicsoftware/CRISPR-Cas9_regorafenib_2024) for file and table formatting.

A nextflow-based nf-core pipeline nf-core/crisprseq (version 2.0.0 https://nf-co.re/crisprseq/2.0.0) was used for screen analysis. For knockout screens, Log_2 fold changes from both drug and DMSO replicates compared to the plasmid reference and corresponding reads from CRISPR-Cas9 knockout studies were corrected for gene-independent effects using crisprcleanR (v3.0.0). Corrected (knockout) or raw read counts were further analyzed using MAGeCK MLE algorithm with MAGeCK software (0.5.9)[33] to identify screen hits. MAGeCK MLE utilizes a maximum-likelihood estimation (MLE) for robust identification of CRISPR-screen hits and assigns beta scores and corresponding FDR statistics to assess gene depletion or enrichment in the screens. Normalization was set to none for knockout screens as crisprcleanR normalizes using the gene wise median of ratios method. In a pairwise manner, screens were compared to either corresponding DMSO controls or plasmid reference as indicated by the design matrices used for MAGeCK MLE (Supplementary Data File 1) for each cell line. To obtain a general trend of all cell lines, the MAGeCK MLE algorithm was used to compare all cell lines treated with regorafenib or DMSO at once to plasmid DNA using corresponding design matrices (Supplementary Data File 1). Screen visualization was generated with MAGeCKFlute (3.16). We further evaluated genes with an FDR < 0.1 when comparing regorafenib versus DMSO control and a beta-value < |0.5| in the comparison of DMSO versus plasmid. For knockout screens, we further excluded essential genes.[34]

Functionally Instructed Compound Library for Drug Screens and Synergy Assays

We searched for drugs interacting with potential genetic modifiers of regorafenib response determined in genome-wide CRISPR-Cas9 screens using the drug gene interaction database (DGIdb). These drugs were then assayed in combination with regorafenib to analyze their potential synergistic effect. For drug combinations, we treated the cells in 4 × 4 matrixes with regorafenib and a second drug following acute cytotoxicity assay protocol. We analyzed the data for synergistic interactions with the R package synergyfinder to calculate zero interaction potential (ZIP) synergy scores for each tested combination in the 4 × 4 matrix and the average across the plate.[35]

RNA Sequencing: Data Analysis and Data Management

RNA sample preparation and data acquisition are outlined in Supplementary information.

Raw sequencing data (fastq files) were analyzed using the nf-core/rnaseq pipeline v3.12.0. The pipeline included trimming of reads (Trim Galore! v0.6.4), alignment to the GRCh37 genome (STAR vSTAR_2.6.1d), and feature quantification (featureCounts v1.6.4). Raw read counts were normalized using DESeq2's median of ratios method.[36] Principal component analyses, including determination of the number of informative components, were performed using the factoextra and stats R packages. For all analyses, we excluded genes that did not show a normalized read count of at least 10 in at least three samples. For differential gene expression between conditions (DMSO or regorafenib) of individual cell lines, we applied Wald statistics using a "design = ~condition" formula. In order to investigate common changes upon regorafenib treatment, we used a "design = ~cell_line + condition" formula, thereby regressing out gene expression changes associated with distinct cell line backgrounds. For differential gene expression changes upon regorafenib between any combination of pairwise cell line comparisons, we used a "design = ~cell_line + condition + cell_line:condition" formula and obtained interaction genes from all possible pairwise comparisons using Wald statistics. The resulting list of potential interaction genes was clustered using the degPatterns function from the DEGreport R package. In order to determine regorafenib-associated gene expression changes and their relation to navitoclax-regorafenib synergy, we first grouped cell lines by the presence of synergy (navitoclax_synergy). We then assessed genes differentially affected by regorafenib treatment alongside this pairwise comparison by employing an interaction term (design = ~condition + navitoclax_synergy + condition: navitoclax_synergy).

DigiWest

DigiWest protein profiling was performed as published[37] (Supplementary Information) using 108 primary antibodies (Supplementary Data File 2). Pathway allocation of analytes was mapped based on the KEGG database.[38] For quantification of the antibody-specific signals, an Excel-based analysis tool was employed[37] that automatically identifies peaks of appropriate molecular weight and calculates the peak area (reported as accumulated fluorescence intensity = AFI). A total of 123 relevant peaks were identified with 90 (73.2%) generating reliable and nonweak signals (>50 AFI). Signal intensity was normalized to the total amount of protein loaded onto the beads (Supplementary Data File 3).

Acute Cytotoxicity Assay and Clonogenic Survival Assay

Assays were performed as previously described[39] and outlined in Supplementary information.

qRT-PCR

After 72 h treatment, we harvested the cells, isolated RNA, transcribed RNA to cDNA, and performed qPCR (Supplementary Information).

Genetic Validation of CRISPR Screen Hits

We selected genes which were enriched in the CRISPR-Cas 9 genome-wide activation screens (see below). Subsequently, one of the sgRNAs targeting these genes from the Calabrese library was cloned as oligo duplex into the pXPR_502 vector (gift from John Doench & David Root (RRID:Addgene_96923; https://scicrunch.org/scicrunch/data/record/nif-0000-11872-1/Addgene_96923/resolver?q=pXPR_502&l=pXPR_502&i=rrid:addgene_96923)) using NEBridge Golden Gate Assembly Kit (BsmBI-v2) (New England Biolabs, Inc., Ipswich, MA, USA). For generation of CRISPR knockout cell lines, we used sgRNAs targeting genes which were depleted in our knockout screens (see below) from the Brunello library and cloned them into the lentiGuide-Puro vector (gift from Feng Zhang (RRID:Addgene_52963; https://scicrunch.org/scicrunch/data/record/nif-0000-11872-1/Addgene_52963/resolver?q=lentiGuide-Puro&l=lentiGuide-Puro&i=rrid:addgene_52963)) using BsmBI-v2 (New England Biolabs, Inc., Ipswich, MA, USA). We produced lentiviral particles containing the different activation or knockout plasmids with corresponding empty vector control plasmids, transfected dCas9-VP64 (activation) or Cas9 (knockout) expressing glioma cell lines and selected with the same puromycin concentrations as in the CRISPR screens.

Immunoblot

Immunoblot analyses were performed as previously published.[39,40] Primary antibodies are listed in Supplementary information.

Glioma Cell Lines and Glioma Stem-Like Cell Cultures

We used LN18, LN229, LNZ308, T98G, SMA560 glioma cell lines and glioma stem-like neurosphere GS-2 and GS-9 cell lines (Supplementary Information).

Primary Glioblastoma Cultures

Primary cultures were generated[40] and treated as indicated. Bliss Independence Criterion was used to evaluate synergism potential. We calculated a predicted value for additivity, the product of the two monotherapies, and compared it with the observed measurement of combination treatment. Lower observed values compared to the prediction indicate towards synergy.[41]

Patient-Derived Microtumors and Co-culturing with Autologous Tumor-Infiltrating Lymphocytes

Generation of patient-derived microtumors (PDMs) from residual material of freshly resected glioblastoma tissue was accomplished as previously described[39,40,42–44] (Supplementary Information).

Orthotopic Murine Glioma Models

We injected 5×10^6 SMA560 glioma cells or 75×10^6 LN229 or 150×10^6 GS-2 cells into the right striatum of VM/Dk mice[45] or CD1nu/nu mice, respectively[39,44,46] (Supplementary Information).

Ethics Statement

The ethics committee of the University Hospital Tübingen approved the use of patient samples (610/2020BO and 225/2023 BO2). Approval for animal experiments was granted by the Tübingen regional council and conducted in compliance with animal welfare regulations.

Statistical Analysis

We used two-way ANOVA for statistical analysis of clonogenic survival assays and one-way ANOVA for qPCR and cytotoxicity on PDMs with and without tumor-infiltrating lymphocytes (TILs) results. For the treatment of CRISPR cell lines in comparison with the respective empty vector control, we used paired *t*-test. All replicates are derived from distinct samples and Gaussian distribution of all samples was assumed and respective post hoc analysis for multiple comparisons were used. For DigiWest analysis, the Wilcoxon Rank-Sum test was used for differential expression analyses, and the Mann–Whitney *U* test was used for all other comparisons between groups unless stated otherwise. We assumed an adjusted p-value below 0.05 as statistically significant. In all graphs, we show mean ± SD, normalizations are indicated in figure legends. We performed a biostatistical assessment for the animal experiments. We aimed in the sample size planning for a power of 80%, assuming normal distribution and standard deviation based on previous experiments for the time until onset of neurological symptoms. We used

Gehan–Breslow–Wilcoxon test or Log-rank test as stated in the figure legends for survival analysis.

Results

Functional Genomics-Based Discovery of Potential Modifiers of Regorafenib

We performed CRISPR-Cas9 activation (Calabrese library) and knockout screens (Brunello library) under regorafenib employing glioma using in vitro models capable of generating the cell number necessary for genome-wide screening (Figure 1A). We used five different glioma and glioma stem-like cell lines GS-9, LN229, LN18, LNZ308, and T98G, covering different genetic backgrounds including *MGMT* gene promoter methylation status. All cell lines express variable combinations of tyrosine kinases targeted by regorafenib: VEGFR1 is expressed in LN229, VEGFR2 is expressed in LNZ308, RET is expressed in GS-9, PDGFR-β is highly expressed in LNZ308, LN18, and T98G (Supplementary Figure S1). Furthermore, an interrogation of publicly available single-cell RNA sequencing data sets revealed distinct expression patterns of regorafenib targets in the tumor cell compartment and in the microenvironment, including high presence of PDGFRA, BRAF, and FGFR1 in all 4 cellular glioma states (Supplementary Figures S2–S5).[47,48] Regorafenib is cytotoxic in all cell lines and induces target regulation (Supplementary Figures S6 and S7). We fine-tuned regorafenib concentrations for each cell line to achieve cytotoxic or cytostatic effects in order to prioritize resistance (activation) or synthetic lethal (knockout) screen hits, respectively. Screens were analyzed using MAGeCK MLE to discover screen hits both in single cell lines and hits that uniformly scored across distinct cell lines (Supplementary Data Files S4 and S5).

Both activation and knockout screens showed high sgRNA mapping ratios and clustering in line with experimental conditions, indicating good screening performance (Supplementary Figures S8, S9A and B). For knockout screens, we extended these low-level quality metrics and also assessed the correction of gene-independent effects in CRISPR knockout screens as well as the depletion of well-known common essential genes. These analyses provided evidence for successful segmental correction in genomic regions with copy number gains and revealed strong depletion of common essential genes, indicating good screen performance of the knockout screens (Supplementary Figure S9).

By focusing on uniformly scoring genes, we identified hits that might modify cellular response to regorafenib throughout the different genetic backgrounds of the cell lines. We focused on those genetic hits that were selected for either positively or negatively in regorafenib-treated samples but not in corresponding DMSO treatment arms. Among the potential modifiers of drug response in distinct glioma cell lines in activation screens (Calabrese library) (Figure 1B), we identified in total 16 positively and 22 negatively selected genes upon regorafenib. Among the positively selected genes, we identified B-cell lymphoma 2 (*BCL2*) family members BCL2 and BCL2 like 1 (*BCL2L1*), integrin subunit beta 3 (*ITGB3*), *ITGB5*, and erb-b2 receptor tyrosine kinase 3 (*ERBB3*). Two of these positively selected activation screen hits, *BCL2* and *BCL2L1*, were positively selected in the four cell lines GS-9, LN18, LN229, and T98G but not in LNZ308 (Supplementary Figure S10). Negatively selected genes in activation screens included dual specificity phosphatase 9 (*DUSP9*) and protein tyrosine phosphatase nonreceptor type 7 (*PTPN7*).

For knockout screens, we used GS-9 and LN229 cell lines, representatives of glioma stem-like and long-term cell lines (Figure 1C; Supplementary Figure S11). Genes that were negatively selected in the regorafenib condition but not regulated in DMSO-treated samples were defined as potential synthetic lethal interactors to regorafenib. In total, we identified 51 negatively selected genes in the uniform analysis across glioma cell lines. These include A-Raf (*ARAF*), mitogen-activated protein kinase kinase 1 (*MAP2K1*), and phospholipase C epsilon 1 (*PLCE1*). Positively selected genes across distinct glioma cell lines were 185, among them *DUSP6*, ubiquitin conjugating enzyme E2 D3 (*UBE2D3*), and neurofibromatosis 1 (*NF1*).

For GS-9 and LN229, we compared the results of activation and knockout screens. We detected an opposed effect for selected genes (Supplementary Figure S12). For example, a gene that is depleted in the GS-9 knockout screen while enriched in the activation screen is *PLCE1*, whereas *DUSP6* is in both cell lines enriched in the knockout screens and depleted in the activation screens.

Using Kyoto Encyclopedia of Genes and Genomes (KEGG) analyses involving all positively or negatively selected genes (red or blue populations in scatter plots in Figure 1B and C) via gProfiler,[49] we identified nuclear factor kappa B (NF-κB) signaling upon the genes positively selected (Figure 1D) and MAPK signaling upon the negatively selected genes in activation screens (Figure 1E). Furthermore, we identified pathways associated with aminoacryl-tRNA biosynthesis, ribosomal formation, thermogenesis, and ubiquitin mediated proteolysis via potential genetic modifiers derived from positively selected genes identified in knockout screens (Figure 1F) as well as pathways with various functions from the negatively selected genes, i.e. interaction between cells or cells with extracellular matrix, intracellular signaling, like ErbB, hypoxia-inducible factor 1 (HIF-1), or Ras-related protein 1 (Rap1) pathways, or immune regulation (Figure 1G).

We performed a genetic validation of selected sgRNAs from activation (*BCL2*, *BCL2L1*, *FOXC1*, *SERAC1*) and knockout libraries (ARAF), and sgRNAs from the Calabrese library increased protein levels for screen candidates including Bcl-2 and Bcl-x_L (Supplementary Figures S13A and S14A), while sgRNAs from the Brunello library led to a decrease in protein levels (Supplementary Figures S13B and S14B). Furthermore, gain-of-function of *BCL2* significantly attenuated the cytotoxic effect of regorafenib (Supplementary Figure S13C), while loss-of-function of *ARAF* sensitized glioma cells for regorafenib (Supplementary Figure S13D).

Pharmacological Validation of Potential Interactors of Regorafenib-Mediated Antiglioma Effects In Vitro

We performed a pharmacological validation of selected hits that were positively or negatively selected in regorafenib-treated samples. Based on an interrogation of the drug

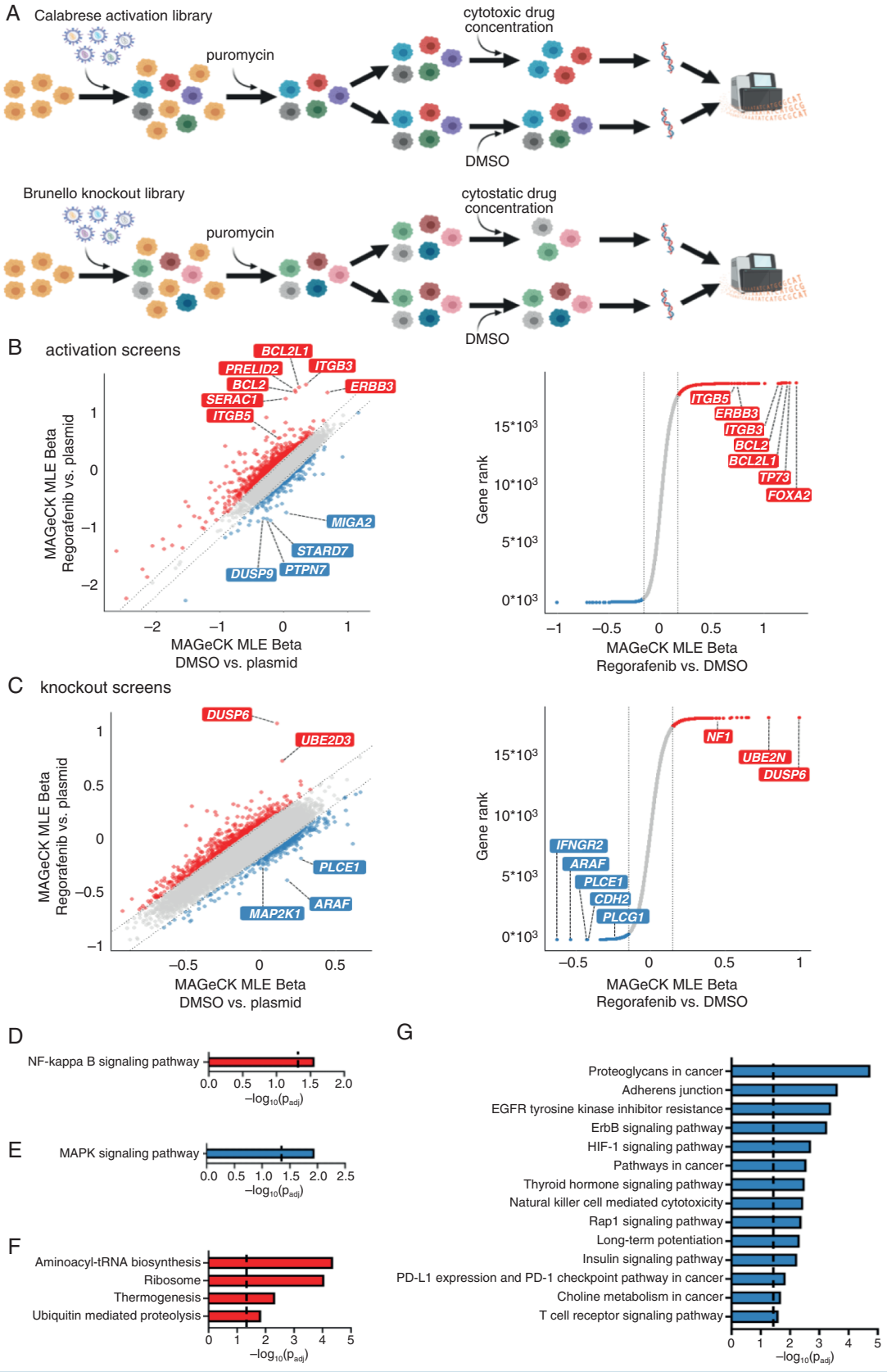

Figure 1. CRISPR-Cas9 activation and knockout screens. (A) Schematic presentations of CRISPR-Cas9 activation and knockout screens. (B), CRISPR-Cas9 activation screen analysis modeled across five glioma cell lines. Left: scatter plot of MAGeCK MLE results comparing Calabrese sgRNA distributions from regorafenib- or DMSO-treated cells to the plasmid library. Right: Rankview plot illustrating with the comparison of

regorafenib- versus DMSO-treated samples. (C) CRISPR-Cas9 knockout screen analysis modeled across two glioma cell lines. Left: Scatter plot comparing Brunello sgRNA distributions of regorafenib- or DMSO-treated cells versus the plasmid control. Right: Rankview plot comparing the regorafenib- versus DMSO-treated samples. (D–G) KEGG pathways significantly affected by positively (D, F) or negatively selected (E, G) genes, dotted line indicates P_{adj} of .05, (D) and (E) display CRISPR-Cas9 activation screens and (F) and (G) display CRISPR-Cas9 knockout screens. All indicated genes score at FDR < 0.1 in the comparison of regorafenib versus DMSO treatment.

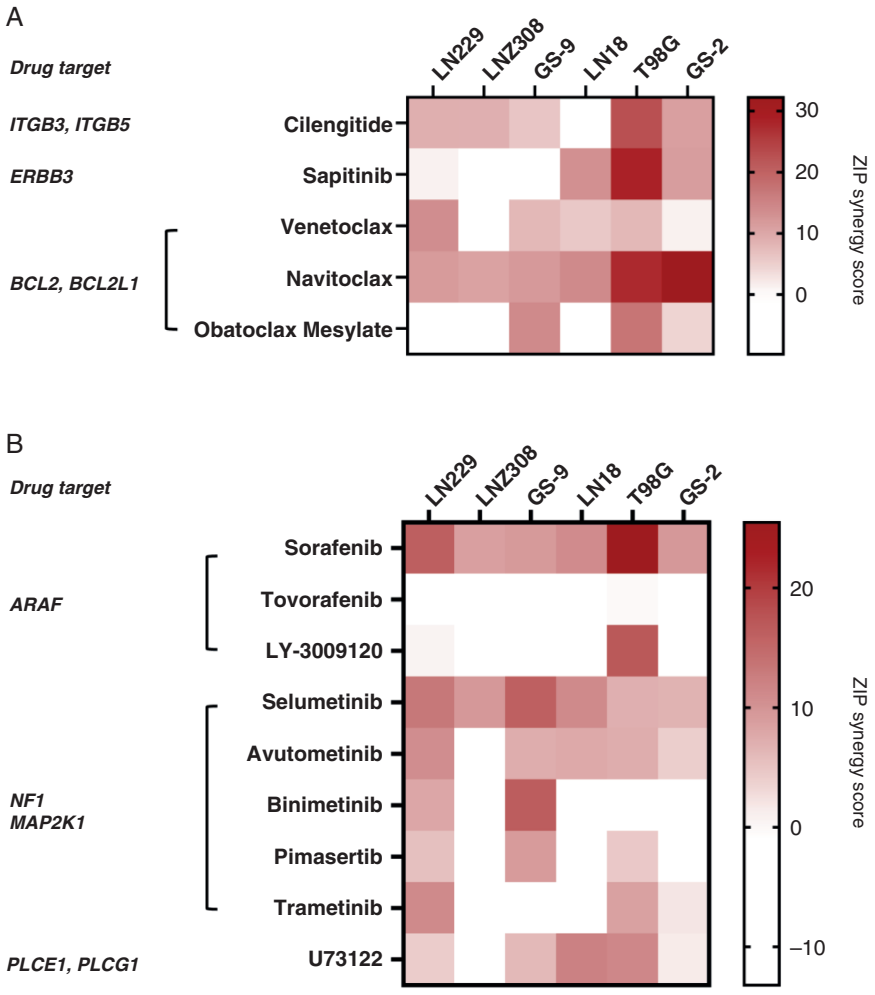

Figure 2. Drug synergy assays. Combination treatment of regorafenib with drugs targeting functionally instructed modifiers in human glioma cell lines after 72 h treatment (n = 2). For each drug the target identified in the CRISPR-Cas9 activation (A) or knockout screen (B) is indicated on the left.

gene interaction database (DGIdb), we selected 14 drugs (Supplementary Table S1) targeting potential molecular modifiers, five of them targeting *BCL2*, *BCL2L1*, *ERBB3*, *ITGB3*, and *ITGB5* gene products identified in activation screens (cilengitide, sapitinib, venetoclax, navitoclax, and obatoclax mesylate), and nine drugs targeting *ARAF*, *MAP2K1*, *PLCE1*, and *PLCG1* gene products identified in knockout screens (sorafenib, tovorafenib, LY-3009120, selumetinib, avutometinib, binimetinib, pimasertib, trametinib, U73122).

Next, we analyzed different combination therapies involving regorafenib with one of these compounds in six distinct glioma cell culture models, employing a maximum of IC_{50} monotherapy concentrations as determined by dose–response curves (concentrations per cell lines listed in Supplementary Table S1). We performed "synergy assays" combining each of these compounds with regorafenib and evaluated their synergistic potential using the zero interaction potency (ZIP) model[35] of drug synergy (Figure 2; Supplementary Fig. S15–S28). We detected the strongest synergistic effects in the combination of regorafenib with the Bcl-2 family inhibitor navitoclax, the integrin antagonist cilengitide, the Raf and multi kinase inhibitor sorafenib, and the mitogen-activated

protein kinase kinase 1/2 (MEK1/2) inhibitor selumetinib (Figure 2). Bcl-2 family inhibitor navitoclax displayed synergistic antiglioma effects with regorafenib in all cell lines (Figure 2A; Supplementary Figure S15). Venetoclax, targeting Bcl-2, and obatoclax mesylate, targeting Bcl-2 and Bcl-x_L were synergistic in four (GS-9, LN18, LN229, LNZ308) or three (GS-2, GS-9, T98G) cell lines, respectively (Figure 2A; Supplementary Figure S16 and S17). Integrin inhibitor cilengitide plus regorafenib were a synergistic combination in all cell lines except of LN18 (Figure 2A; Supplementary Figure S18). For the combination of regorafenib with sorafenib, a multi-kinase RAF inhibitor, we detected a synergistic effect throughout all cell lines (Figure 2B; Supplementary Figure S19). The synergistic effect for combining regorafenib with selumetinib, targeting MEK1/2, was most effective in LN229, LNZ308, GS-9, and LN18 cell lines (Figure 2B; Supplementary Figure S20).

We then performed clonogenic survival assays for the combination of regorafenib with navitoclax, cilengitide, sorafenib, selumetinib, venetoclax, or trametinib (Figure 3; Supplementary Figures S29–S32). In LN229 cells, combinations of regorafenib with cilengitide or selumetinib significantly reduced clonogenic survival compared to respective monotherapies. In LN18 cells, combinations of regorafenib with navitoclax or selumetinib were significantly more effective than the monotherapies. The combination treatments of regorafenib with navitoclax, venetoclax, sorafenib, or trametinib significantly reduced clonogenic survival in LN229 cells only compared to regorafenib monotherapy. In LN18 cells, the combination of regorafenib with cilengitide was not synergistic.

Functionally Instructed Combination of Regorafenib and Navitoclax Is Synergistic Ex Vivo

We next investigated the efficacy of selected combination therapies in primary glioblastoma cultures (TUE-PC1, TUE-PC2, TUE-PC3, TUE-PC6, TUE-PC14, TUE-PC15, and TUE-PC16) ex vivo (Figure 4A). We treated TUE-PC1, TUE-PC2, TUE-PC3, TUE-PC6, TUE-PC14, TUE-PC15, and TUE-PC16 in acute cytotoxicity assays with different concentrations of regorafenib ranging from 2.5 μM to 15 μM and detected a cytotoxic effect of regorafenib on all samples (Supplementary Figure S33A). Treatment with mono- and combination therapies of regorafenib (7.5 μM) with navitoclax (2.5 μM) or selumetinib (2.5 μM) (Figure 4B; Supplementary Figure S33B and D) led to a synergistic interaction based on evaluation of the matching statistical model Bliss Independence Criterion.

Synergistic Interaction of Regorafenib Treatment with Bcl Family Inhibition Is Mediated by Regorafenib-Induced CCR1 Downregulation

We performed qPCR and immunoblot analysis after regorafenib treatment and identified an upregulation of *BCL2* mRNA expression after 72 hours in all cell lines. This was further confirmed by immunoblots and immune cytochemistry (Supplementary Figures S34 and S35).

We next performed mRNA sequencing (Supplementary Figure S36A). The vast majority of regorafenib-induced alterations were associated with cell line-specific gene expression changes (Supplementary Figure S36B andC). Based on pairwise comparisons for each model, we identified a median of 1,411 genes (range 846–2,095) to be deregulated by regorafenib (Supplementary Data File 6), and 1,245 to be commonly deregulated upon regorafenib across all cell lines (Supplementary Figure S36D). Genes commonly depleted across cell lines were significantly enriched for different membrane-to-nucleus signaling cascades and indicated a general blockade of cell cycle progression, DNA replication, and transcription (Supplementary Figure S36E and F).

Using an interaction term to describe cell line-specific effects of regorafenib, we identified a total of 1,440 unique genes that were differentially regulated by regorafenib across all potential pairwise comparisons of cell lines, with the majority of those genes being deregulated in only a single cell line (Supplementary Figure S37A). In line with these results, we found only a small overlap of deregulated genes across all four cell lines (Supplementary Figure S37B). However, we found a highly homogenous response to regorafenib in GS-9, LN18, and LN229 cells when using gene set enrichment analyses, particularly for downregulated genes, which was phenotypically distinct from enrichments that we found in LNZ308 cells (Figure 5A; Supplementary Figure 37C). We correlated baseline mRNA expression profiles with these differential regorafenib effects. Indeed, LNZ308 cells displayed a distinct gene expression pattern (Supplementary Figure 38A–D), e.g., regorafenib target genes *KDR*, *c-Kit,* and *PDGFRB* were only expressed in LNZ308 (Supplementary Fig. 38E), suggesting differing target engagement upon regorafenib treatment. Furthermore, LNZ308 displayed a unique expression pattern of cell cycle progression regulators, with *CDKN2A* being the top gene upregulated in LNZ308 as compared to other glioma cell models. Of note, *CDKN1A*, a cell cycle inhibitor closely related to *CDKN2A*, is involved in regulating cellular sensitivity to regorafenib.[28] Thus, different *CDKN2A* expression might contribute to different regorafenib sensitivity, too. A DigiWest protein profiling analysis with selected antibodies (Supplementary Data File S2) revealed a broad range of downstream regulation upon regorafenib (Supplementary Figure 39; Supplementary Data File 3) and A-Raf-pS299 was commonly enriched under treatment in all cell lines.

Next, we compared regorafenib-induced mRNA expression profiles of LNZ308 cells versus the other three glioma cell lines (Figure 5A and B). We detected a significant difference between LNZ308 and the other cell lines regarding activation of different intracellular pathways, including regulation of RAF isoforms, DUSP6, DUSP9, phosphorylation of RAF isoforms, MEK1, Akt, PDGFRβ, and PP1 alpha, which matches with RNAseq data. As these RNAseq enrichment results validated in DigiWest closely correlated with our results for BCL family members from CRISPR screening, we specifically investigated differences in regorafenib effects in LNZ308 cells as compared to all other cell lines, identifying 218 genes to be differentially regulated (Figure 5C). Among the top regulated mRNAs, we found chemokine receptor 1 (*CCR1*), a gene known to

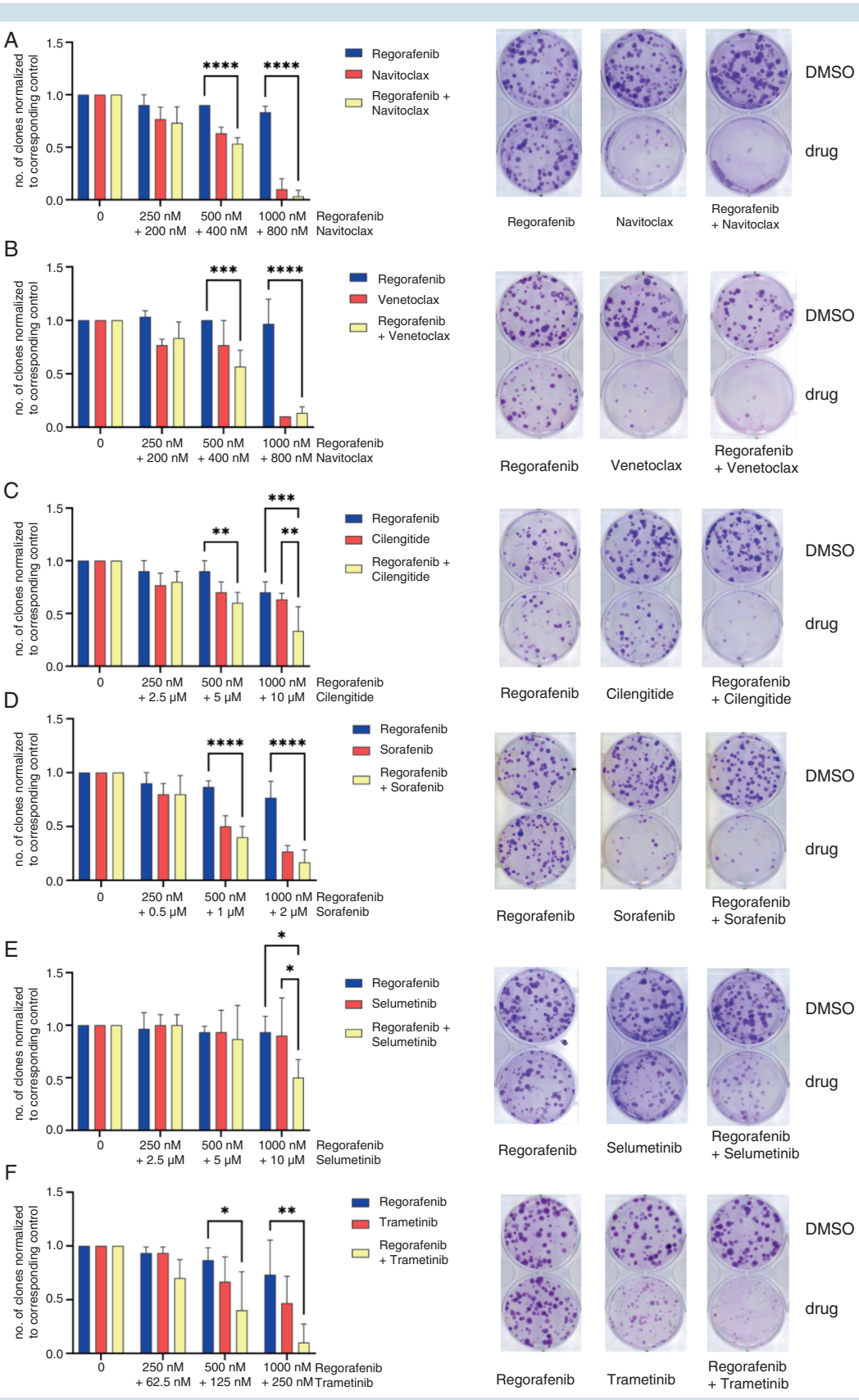

Figure 3. Clonogenic survival upon combination treatments. Evaluation of selected drugs in combination with regorafenib in clonogenic survival assays in LN229 cells: regorafenib in combination with (A) navitoclax, (B) venetoclax, (C) cilengitide, (D) sorafenib, (E) selumetinib, and (F) trametinib. Left: bar graph ($n = 3$), statistical analysis: two-way ANOVA, right: representative plates for highest treatment concentrations. *$P_{adjust} < .05$, **$P_{adjust} < .01$, ***$P_{adjust} < .001$, ****$P_{adjust} < .0001$, only significant differences are indicated (please note that bars in A-C are structured as follows: first column: regorafenib monotherapy, second column; second drug monotherapy, third column: combination therapy).

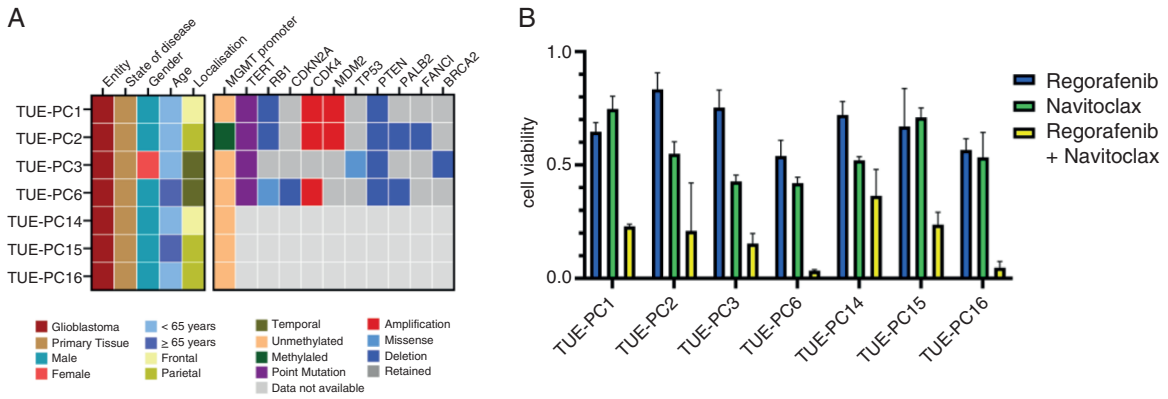

Figure 4. Regorafenib plus navitoclax ex vivo. (A) Clinical (left panel) and molecular (right panel) features of primary tumors. (B) Primary glioblastoma cultures treated with monotherapy and combination treatment of regorafenib (7.5 μM) and navitoclax (2.5 μM) normalized to untreated control. $n = 1$ for each tumor sample due to limited availability, standard deviation based on technical triplicates (Please note that the structure of the columns in B is as follows: first column: regorafenib monotherapy, second column: navitoclax monotherapy, third column: regorafenib + navitoclax).

be downregulated by overexpression of BCL2,[50] to be consistently downregulated by regorafenib in GS-9, LN18, and LN229 cells, while *CCR1* levels were unaffected in LNZ308 cells (Figure 5D). Thus, regorafenib phenocopies the effects of BCL2 overexpression in a cell line-specific manner, which might be related to its synergistic action together with navitoclax. Furthermore, single-cell RNA sequencing analyses from publicly available data sets[47,48] revealed BCL2L1 and BCL2 expression in several cell types and across different glioma cellular states. CCR1 was detected on intratumoral myeloid cells and on distinct glioma cells (Supplementary Figure S40).

Furthermore, the selective CCR1 inhibitor BX471 in combination with navitoclax synergistically inhibited growth of all glioma cell models (Figure 5E), whereas CCR1 overexpression in glioma cells significantly diminished the synergism of regorafenib and navitoclax (Supplementary Figures S41 and S42). These data suggest that regorafenib-mediated downregulation of CCR1 is functionally relevant for synergistic activity alongside inhibition of Bcl family members.

Functionally Instructed Combination of Regorafenib and Navitoclax Prolongs Survival In Vivo

Finally, we investigated combinations involving regorafenib in three orthotopic mouse models, one syngeneic immunocompetent model (SMA560/VM/Dk glioma) and two xenograft models (LN229 or glioma stem-like GS-2 cells in immunodeficient CD1 nude mice) (Figure 6A–C; Supplementary Figures S43–S45).

In the SMA560/VM/Dk model the regorafenib plus navitoclax treatment group did not reach the median during the observation period of 120 days (Figure 6A). The survival was prolonged compared to navitoclax monotherapy, solvent treatment and regorafenib monotherapy (Figure 6A). Regorafenib plus navitoclax also significantly prolonged survival in LN229 (Figure 6B) and in GS2-bearing mice (Figure 6C).

Immunohistochemical analyses revealed that CD11b and CD204 were qualitatively reduced (Figure 6D) suggesting a treatment-related effects on the myeloid compartment. CD4 and CD8 were modestly enhanced after regorafenib (Figure 6D), while VEGFR2 and CD31 were qualitatively reduced (Supplementary Figure S43A and B). In an ex vivo model, regorafenib-mediated cytotoxicity in PDMs was increased in the presence of autologous TILs (Supplementary Figure S44C (1–2)) further supporting a regorafenib-related effect on the immune compartment.

Based on the synergistic antiglioma effects of regorafenib plus cilengitide in vitro (Figures 2A and 3C), we also investigated the combination of regorafenib with cilengitide in the orthotopic LN229/CD1 nude mouse model (Supplementary Figure S18G). Regorafenib plus cilengitide significantly prolonged survival compared with regorafenib monotherapy, but rather modest. Furthermore, the combination was not superior to cilengitide monotherapy.

Discussion

Options for systemic therapies in glioblastoma, particularly for progressive disease are limited.[51] Our aim here was to provide biological rationales for future clinical trials. We focused on identifying combinations therapies involving regorafenib. Although bevacizumab is registered in some countries, the spectrum of RTKs that are inhibited by regorafenib is broader. Furthermore, it is an oral compound facilitating the clinical application in an outpatient setting.

Combination therapies involving regorafenib require biological rationales. In our study, we discovered *BCL2* and *BCL2L1* as promising targets in this regard (Figure 1B; Supplementary Figure S10). *BCL2* and *BCL2L1* are upregulated upon regorafenib (Supplementary Figure 34),

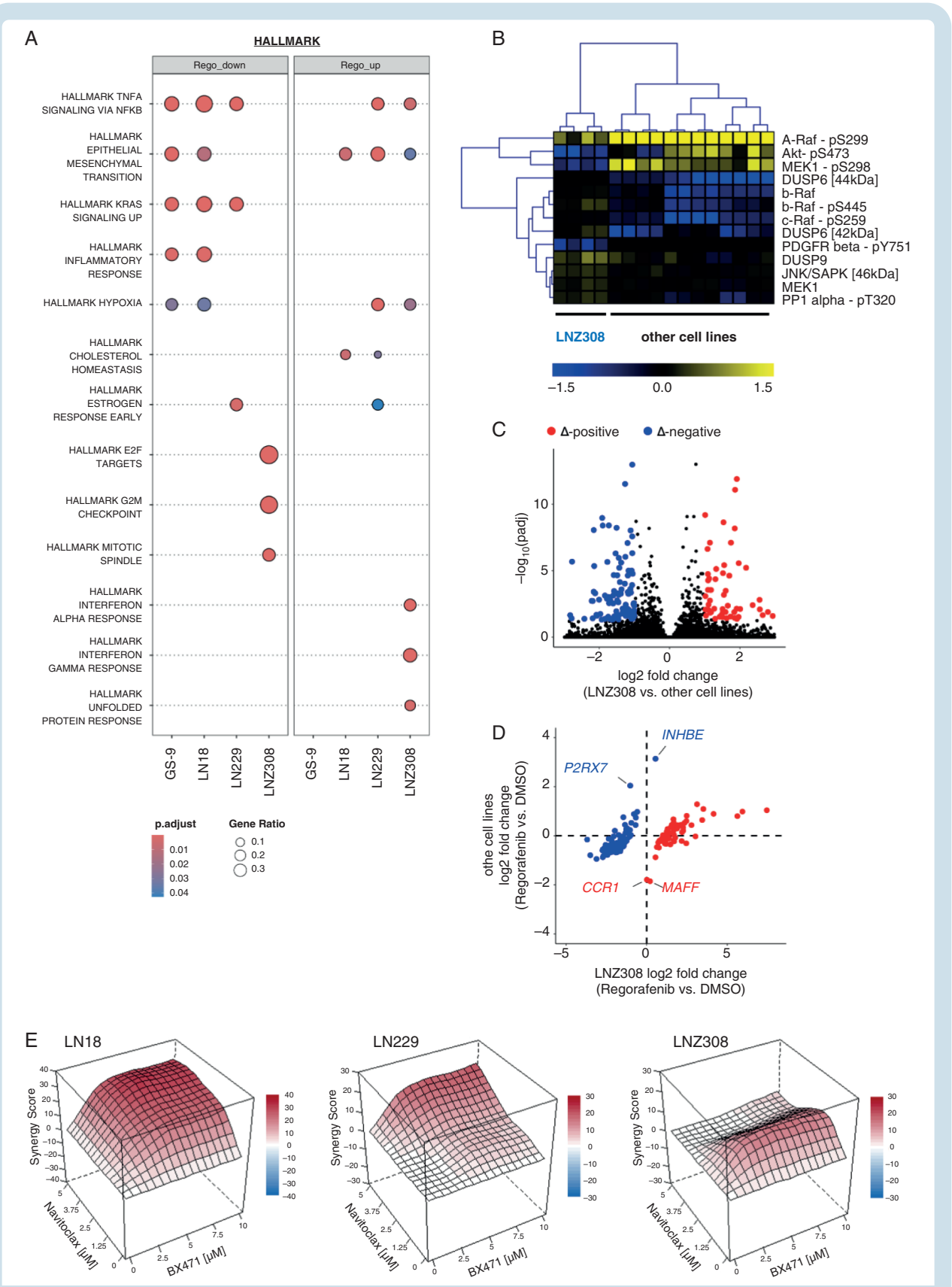

Figure 5. Regorafenib-induced molecular alterations. (A) DigiWest protein profiling heatmap containing comparison of protein expression of LNZ308 versus three other glioma cell lines (GS-9, LN18, LN229). (B) RNAseq-based gene set enrichment analysis on genes regulated upon regorafenib treatment in four glioma cell lines. Both analyses show a more uniform regulation under regorafenib treatment in GS-9, LN18, and LN229 as compared to LNZ308. (C) Volcano plot illustrating genes differentially affected in LNZ308 cells as compared to three other glioma cell

lines (GS-9, LN18, LN229) upon regorafenib treatment for 24 h. (D) Scatter plot showing actual gene expression changes in LNZ308 or all other glioma cell lines for genes differentially regulated upon regorafenib treatment. Note the exclusive downregulation of the BCL2 target chemokine receptor 1 (CCR1) in GS-9, LN18, and LN229 cells upon regorafenib treatment, while CCR1 expression is unchanged in LNZ308 cells. (E) Synergy assays in LN18, LN229, and LNZ308 using the selective CCR1 antagonist BX471 in combination with navitoclax reveal synergistic interaction of CCR1 and Bcl family inhibition. The scale bars indicate ZIP synergy score values.

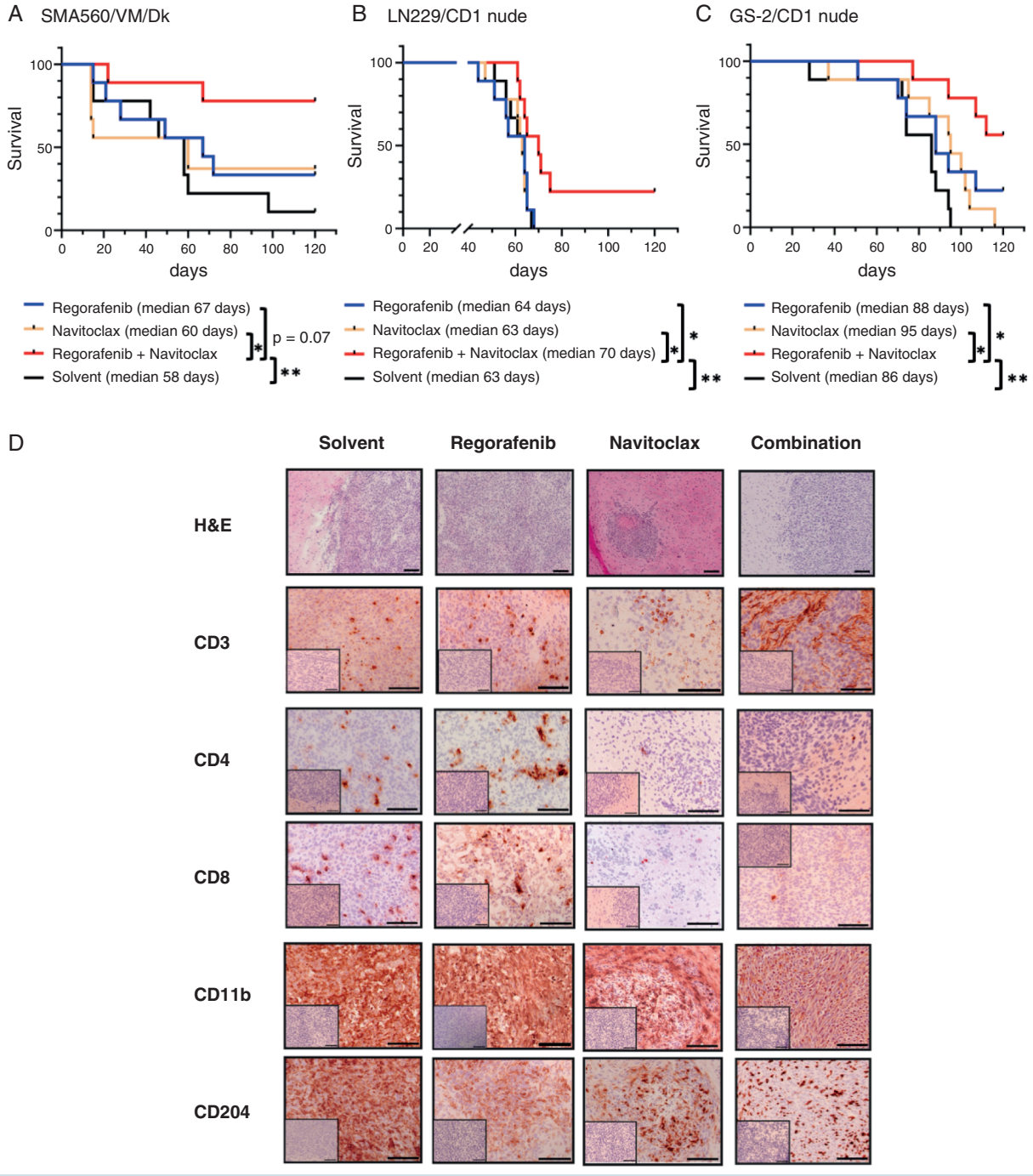

Figure 6. Regorafenib plus navitoclax in vivo. (A–C) Kaplan–Meier curve of VM/Dk transplanted with SMA560 (A) and CD1 nude mice transplanted with either LN229 (B) or GS-2 cells (C) upon treatment with regorafenib, navitoclax, the combination of regorafenib and navitoclax, and solvent control ($n = 9$). For regorafenib and navitoclax combination in SMA560/VM/Dk and GS-2/nude models no median was reached. Statistical analysis with Gehan–Breslow–Wilcoxon test, comparisons between monotherapies or monotherapy versus solvent control are not significantly different and p-values are not indicated in the figure. (D) Immunohistochemical staining in SMA560/VM/Dk post-treatment tissues. First row, representative H&E stainings. Second to 6th row, representative IHC staining patterns of tumor tissues with indicated antibodies. Small inserts display staining control without application of primary antibody. Scale bars 100 µm. $^{*}P_{adjust} < .05$, $^{**}P_{adjust} < .01$, $^{***}P_{adjust} < .001$, $^{****}P_{adjust} < .0001$.

and regorafenib plus an inhibition of Bcl2 family members with navitoclax displayed antiglioma synergy in vitro (Figures 2A and 3A, Supplementary Figures S15, 29, 30, and 32), ex vivo (Figure 4B; Supplementary Figure S33) and in three orthotopic glioma models in vivo (Figure 6).

Integrated analyses of mRNA and protein level regulation revealed regorafenib-induced modifications (Figure 5). We identified a downregulation of the chemokine receptor CCR1, a well-known target of BCL2 overexpression,[50] to be strongly correlated with synergistic action of regorafenib and navitoclax. In line with this, we observed a regorafenib-associated modulation of the intratumoral myeloid niche and a reduction of tumor-associated macrophages. CCR1 signaling is relevant for the recruitment of tumor-associated macrophages and maintenance of an immunosuppressive microenvironment.[52,53] Targeting CCR1, also expressed on myeloid cells, led to a reduction of tumor growth and re-composition on the tumor-associated microenvironment in several colon-carcinoma mouse models.[54,55] Regorafenib-induced re-composition of the tumoral myeloid compartment was observed in multiple syngeneic liver cancer model.[56] Furthermore, in vitro data from hepatocellular carcinoma (HCC) displayed a synergistic effect regorafenib plus navitoclax.[57]

The use of glioma cell lines for CRISPR-Cas9 activation and knockout screens might be considered a limitation of our study but was inevitable due to the very high numbers of cells that are required for this functional genomics approach (30×10^6 and 40×10^6 transduced cells per replicate in each condition for activation and knockout screens, respectively) in a 500x coverage. We addressed this limitation by using cell lines with different genetic backgrounds (Supplementary Figure S1) and a comprehensive validation strategy of all functional genomics-based results in several preclinical models in vitro, ex vivo, and in vivo. We identified synergistic interactors of regorafenib, including *ITGB3*, *ITGB5*, *ARAF*, and *MAP2K1* (Figure 1B and C; Supplementary Figures S10 and 11). *ITGB5* expression has been reported in the context of regorafenib resistance in HCC.[58] In vitro, regorafenib plus integrin inhibition via cilengitide displayed synergistic antiglioma effects in all glioma cell lines except of LN18 (Figures 2A and 3C, Supplementary Fig. S18, S29B, S32E-H), due to low levels of ITGB3 protein expression in LN18[59] (mRNA expression: Supplementary Fig. S1). In vivo, regorafenib plus cilengitide displayed statistically significant but rather modest improved survival in the LN229 xenograft model compared with regorafenib monotherapy (Supplementary Figure S18G). Combination treatments of regorafenib with selumetinib led to synergistic effects in vitro and ex vivo (Figures 2B and 3E, Supplementary Figures S20, S29C, S31, S32). In preclinical/experimental HCC models, synergistic combination therapies involving regorafenib included TOP2A inhibition (siRNA, doxorubicin treatment),[60] targeting of sphingosine kinase 2 (SphK2),[61] transforming growth factor β receptor 1 (TGFβ-R1) inhibition,[62] as well as combination with programmed cell death protein 1 (PD-1) blockade.[63] Clinical trials in HCC investigated simultaneous/sequential combination of PD-1 blockade plus regorafenib (e.g., NCT03347292 and NCT04170556). In experimental models of colorectal cancer, strategies for combination therapies involving regorafenib included neurogenic locus notch homolog protein 1 (NOTCH 1) inhibition,[64] myeloid cell leukemia 1 (Mcl-1) inhibition[65] and inhibition of monoacylglycerol lipase (MAGL).[66]

Taken together, our preclinical study provides a biological rationale for combination therapies involving regorafenib in glioblastoma advocating for clinical translation of these preclinical data. Based on our data, we conclude that the functionally-instructed combination of regorafenib with the Bcl-2 family inhibitor navitoclax offers the highest potential to inform the design of a clinical phase I trial.

Supplementary material

Supplementary material is available online at *Neuro-Oncology* (https://academic.oup.com/neuro-oncology).

Keywords

Bcl-2 | Bcl-x_L | experimental glioma | functional genomics | synergy

Funding

Parts of this study were funded by the Adolf-Leuze Stiftung, the Medical Faculty Tübingen (Demonstratorprojekt Personalisierte Medizin and NWG program), Else Kröner Forschungskolleg (2019_Kolleg_14) and the Deutsche Forschungsgemeinschaft (DFG, German Research Foundation), Germany's Excellence Strategy, Cluster of Excellence—EXC 2180 – (390900677).

Conflict of interest statement

Institutional funding was provided to the University Hospital Tübingen for the following activities of GT: GT served on advisory boards (Bayer, Boehringer Ingelheim, CureVac, Miltenyi Biomedicine, Novocure), as a consultant (Bayer, Boehringer Ingelheim, CureVac), as steering committee member in noninterventional trials ONTRK (Bayer) and TIGER (Novocure), as a speaker (Novocure, Servier). Parts of this scientific publication are the subject of (nonpublished) European patent application EP 23 198 443.6, filed with the European Patent Office on 20 September 2023 with GT, LAH, LK, and DJM listed as inventors. Figure 1A was created with BioRender.com.

Acknowledgments

We thank Sarah Hendel, Heike Pfrommer, and Yeliz Donat for excellent technical assistance and David E. Root and his team from the Broad Institute of MIT & Harvard for fruitful discussions.

Author contributions

Methodology: L.A.H., H.B., L.K., M.Z., B.W., F.T., S.E., J.T., S.S., A.S., M.T., E.W., T.S., C.S., N.C., O.R., L.S., S.N., M.C., D.J.M., G.T.; Data acquisition and analysis: L.A.H., H.B., L.K., M.Z., L.S., D.J.M., S.B., G.T.; Visualization: L.A.H., H.B., L.K., M.Z., A.S., L.S., D.J.M.; Conceptualization: D.J.M., G.T.; Project administration and management: S.B., G.T.; Project Supervision: S.N., G.T.; Writing—original draft: L.A.H., G.T.; Writing—review & editing: all authors.

Data availability

All data and codes from this manuscript are available. The data includes CRISPR-Cas9 screen and RNAseq data. Codes are provided via GitHub with the full links provided in the materials and methods sections for CRISPR-Cas9 screen analysis and RNAseq. CRISPR-Cas9 screen data and design matrices for screen analysis are released on figshare.com (https://figshare.com/s/ffb5150188519079ae33). RNAseq data are released on gene expression omnibus under accession number GSE247498 (https://www.ncbi.nlm.nih.gov/geo/query/acc.cgi?acc=GSE247498) and GSE272737 (https://www.ncbi.nlm.nih.gov/geo/query/acc.cgi?acc=GSE272737).

Affiliations

Department of Neurology & Interdisciplinary Neuro-Oncology, University Hospital Tübingen, Hertie Institute for Clinical Brain Research, Eberhard Karls University Tübingen, Tübingen, Germany (L.A.H., H.B., L.K., M.Z., B.W., F.T., S.E., J.T., S.S., L.S., D.J.M., S.B., G.T.); German Cancer Consortium (DKTK), DKFZ Partner Site Tübingen, Tübingen, Germany (L.A.H., S.E., L.S., G.T.); Cluster of Excellence (EXC 2180) "Image-Guided and Functionally Instructed Tumor Therapies", Eberhard Karls University of Tübingen, Tübingen, Germany (L.A.H., H.B., L.K., B.W., F.T., S.E., J.T., S.S., L.S., S.N., D.J.M., S.B., G.T.); Department of Neurosurgery, University Hospital Tübingen, Eberhard Karls University Tübingen, Tübingen, Germany (H.B.); Center for Neuro-Oncology, Comprehensive Cancer Center Tübingen-Stuttgart, Eberhard Karls University Tübingen, Tübingen, Germany (G.T., H.B.); Quantitative Biology Center, Eberhard Karls University Tübingen, Tübingen, Germany (L.K., S.N.); Biomedical Data Science, Department of Computer Science, Eberhard Karls University Tübingen, Tübingen, Germany (L.K., S.N.); Department of Internal Medicine I, University Hospital Tübingen, Tübingen, Germany (M.Z., M.C.); M3 Research Center for Malignome, Metabolome and Microbiome, Faculty of Medicine, Eberhard Karls University Tübingen, Tübingen, Germany (M.Z., L.S., M.C., S.N.); Department of Computer Science, Eberhard Karls University Tübingen, Tübingen, Germany (M.Z., M.C.); Institute of Biomedical Informatics, University Hospital Tübingen, Eberhard Karls University Tübingen, Tübingen, Germany (M.Z., M.C.); NMI, Natural and Medical Sciences Institute, University of Tübingen, Reutlingen, Germany (A.S., M.T., E.W., T.S., C.S.); Institute of Medical Genetics and Applied Genomics, Eberhard Karls University Tübingen, Tübingen, Germany (N.C.)

References

1. Ostrom QT, Price M, Neff C, et al. CBTRUS statistical report: primary brain and other central nervous system tumors diagnosed in the United States in 2015–2019. *Neuro-Oncology.* 2022;24(Suppl 5):v1–v95.
2. Stupp R, Mason WP, van den Bent MJ, et al; European Organisation for Research and Treatment of Cancer Brain Tumor and Radiotherapy Groups. Radiotherapy plus concomitant and adjuvant temozolomide for glioblastoma. *N Engl J Med.* 2005;352(10):987–996.
3. Gilbert MR, Dignam JJ, Armstrong TS, et al. A randomized trial of bevacizumab for newly diagnosed glioblastoma. *N Engl J Med.* 2014;370(8):699–708.
4. Stupp R, Taillibert S, Kanner A, et al. Effect of tumor-treating fields plus maintenance temozolomide vs maintenance temozolomide alone on survival in patients with glioblastoma: a randomized clinical trial. *JAMA.* 2017;318(23):2306–2316.
5. Picca A, Guyon D, Santonocito OS, et al. Innovating strategies and tailored approaches in neuro-oncology. *Cancers (Basel).* 2022;14(5):1124.
6. Qin A, Musket A, Musich PR, Schweitzer JB, Xie Q. Receptor tyrosine kinases as druggable targets in glioblastoma: do signaling pathways matter? *Neurooncol. Adv.* 2021;3(1):vdab133.
7. Chen H, Kuhn J, Lamborn KR, et al. Phase I/II study of sorafenib in combination with erlotinib for recurrent glioblastoma as part of a 3-arm sequential accrual clinical trial: NABTC 05-02. *Neurooncol. Adv.* 2020;2(1).
8. Hainsworth JD, Ervin T, Friedman E, et al. Concurrent radiotherapy and temozolomide followed by temozolomide and sorafenib in the first-line treatment of patients with glioblastoma multiforme. *Cancer.* 2010;116(15):3663–3669.
9. Wick W, Gorlia T, Bendszus M, et al. Lomustine and bevacizumab in progressive glioblastoma. *N Engl J Med.* 2017;377(20):1954–1963.
10. Schmieder R, Hoffmann J, Becker M, et al. Regorafenib (BAY 73-4506): antitumor and antimetastatic activities in preclinical models of colorectal cancer. *Int J Cancer.* 2014;135(6):1487–1496.
11. Abou-Elkacem L, Arns S, Brix G, et al. Regorafenib inhibits growth, angiogenesis, and metastasis in a highly aggressive, orthotopic colon cancer model. *Mol Cancer Ther.* 2013;12(7):1322–1331.
12. Wilhelm SM, Dumas J, Adnane L, et al. Regorafenib (BAY 73-4506): a new oral multikinase inhibitor of angiogenic, stromal and oncogenic receptor tyrosine kinases with potent preclinical antitumor activity. *Int J Cancer.* 2011;129(1):245–255.
13. Wilhelm SM, Carter C, Tang L, et al. BAY 43-9006 exhibits broad spectrum oral antitumor activity and targets the RAF/MEK/ERK pathway and receptor tyrosine kinases involved in tumor progression and angiogenesis. *Cancer Res.* 2004;64(19):7099–7109.
14. Strumberg D, Schultheis B. Regorafenib for cancer. *Expert Opin Investig Drugs.* 2012;21(6):879–889.
15. Liu S, Du Y, Ma H, et al. Preclinical comparison of regorafenib and sorafenib efficacy for hepatocellular carcinoma using multimodality molecular imaging. *Cancer Lett.* 2019;453(1):74–83.
16. Higuchi T, Igarashi K, Yamamoto N, et al. Multikinase-inhibitor screening in drug-resistant osteosarcoma patient-derived orthotopic xenograft mouse models identifies the clinical potential of regorafenib. *Cancer Genomics Proteomics.* 2021;18(5):637–643.
17. Zhao Z, Wu H, Wang L, et al. Exploration of type II binding mode: a privileged approach for kinase inhibitor focused drug discovery? *ACS Chem Biol.* 2014;9(6):1230–1241.
18. Bruix J, Qin S, Merle P, et al; RESORCE Investigators. Regorafenib for patients with hepatocellular carcinoma who progressed on sorafenib treatment (RESORCE): a randomised, double-blind, placebo-controlled, phase 3 trial. *Lancet (London, England).* 2017;389(10064):56–66.

19. Demetri GD, Reichardt P, Kang Y-K, et al; GRID study investigators. Efficacy and safety of regorafenib for advanced gastrointestinal stromal tumours after failure of imatinib and sunitinib (GRID): an international, multicentre, randomised, placebo-controlled, phase 3 trial. *Lancet (London, England).* 2013;381(9863):295–302.
20. Grothey A, Cutsem EV, Sobrero A, et al. Regorafenib monotherapy for previously treated metastatic colorectal cancer (CORRECT): an international, multicentre, randomised, placebo-controlled, phase 3 trial. *Lancet.* 2013;381(9863):303–312.
21. Lombardi G, De Salvo GL, Brandes AA, et al. Regorafenib compared with lomustine in patients with relapsed glioblastoma (REGOMA): a multicentre, open-label, randomised, controlled, phase 2 trial. *Lancet Oncol.* 2019;20(1):110–119.
22. Werner J-M, Wolf L, Tscherpel C, et al. Efficacy and tolerability of regorafenib in pretreated patients with progressive CNS grade 3 or 4 gliomas. *J Neurooncol.* 2022;159(2):309–317.
23. Lombardi G, Caccese M, Padovan M, et al. Regorafenib in recurrent glioblastoma patients: a large and monocentric real-life study. *Cancers.* 2021;13(18):4731.
24. Rudà R, Bruno F, Pellerino A, et al. Observational real-life study on regorafenib in recurrent glioblastoma: does dose reduction reduce toxicity while maintaining the efficacy? *J Neurooncol.* 2022;160(2):389–402.
25. Tzaridis T, Gepfner-Tuma I, Hirsch S, et al. Regorafenib in advanced high-grade glioma: a retrospective bicentric analysis. *Neuro-Oncology.* 2019;21(7):954–955.
26. Wen P, Alexander B, Berry D, et al. CTNI-85. GBM agile platform trial for newly diagnosed and recurrent GBM: results of first experimental arm, regorafenib. *Neuro-Oncology.* 2023;25(Supplement_5):v97–v98.
27. Caccese M, Desideri I, Padovan M, et al. Association between thyroid function and regorafenib efficacy in patients with relapsed wild-type IDH glioblastoma: a large multicenter study. *J Neurooncol.* 2023;163(2):377–383.
28. Santangelo A, Rossato M, Lombardi G, et al. A molecular signature associated with prolonged survival in glioblastoma patients treated with regorafenib. *Neuro-Oncology.* 2021;23(2):264–276.
29. Padovan M, De Salvo G, Cerretti G, et al. OS09.2.A regorafenib in combination with temozolomide with or without radiotherapy in patients with newly diagnosed MGMT-methylated, IDH wildtype glioblastoma: a phase I dose-finding study (REGOMA-2, EUDRA CT N° 2021-001604-15). *Neuro-Oncology.* 2023;25(Supplement_2):ii20–ii20.
30. Simonelli M, Caccese M, Larrieu-Ciron D, et al. CTIM-32. A parallel cohort phase 2 study of regorafenib plus nivolumab for recurrent or metastatic solid tumors: results in patients with glioblastoma multiforme (GBM) or anaplastic astorcytoma (AA). *Neuro-Oncology.* 2023;25(Supplement_5):v69–v70.
31. Sanson KR, Hanna RE, Hegde M, et al. Optimized libraries for CRISPR-Cas9 genetic screens with multiple modalities. *Nat Commun.* 2018;9(1):5416.
32. Doench JG, Fusi N, Sullender M, et al. Optimized sgRNA design to maximize activity and minimize off-target effects of CRISPR-Cas9. *Nat Biotechnol.* 2016;34(2):184–191.
33. Li W, Xu H, Xiao T, et al. MAGeCK enables robust identification of essential genes from genome-scale CRISPR/Cas9 knockout screens. *Genome Biol.* 2014;15(12):554.
34. Hart T, Brown KR, Sircoulomb F, Rottapel R, Moffat J. Measuring error rates in genomic perturbation screens: gold standards for human functional genomics. *Mol Syst Biol.* 2014;10(7):733.
35. He L, Kulesskiy E, Saarela J, et al. Methods for high-throughput drug combination screening and synergy scoring. In: von Stechow L, ed. *Cancer Systems Biology: Methods and Protocols.* New York, NY: Springer New York; 2018:351–398.
36. Love MI, Huber W, Anders S. Moderated estimation of fold change and dispersion for RNA-seq data with DESeq2. *Genome Biol.* 2014;15(12):550.
37. Treindl F, Ruprecht B, Beiter Y, et al. A bead-based western for high-throughput cellular signal transduction analyses. *Nat Commun.* 2016;7(1):12852.
38. Kanehisa M, Goto S. KEGG. Kyoto encyclopedia of genes and genomes. *Nucleic Acids Res.* 2000;28(1):27–30.
39. Walter B, Canjuga D, Yüz SG, et al. Argyrin F treatment-induced vulnerabilities lead to a novel combination therapy in experimental glioma. *Ad Therapeutics.* 2021;4(9):2100078.
40. Walter B, Hirsch S, Kuhlburger L, et al. Functionally-instructed modifiers of response to ATR inhibition in experimental glioma. *J Exp Clin Cancer Res.* 2024;43(1):77.
41. Yan H, Zhang B, Li S, Zhao Q. A formal model for analyzing drug combination effects and its application in TNF-α-induced NFκB pathway. *BMC Syst Biol.* 2010;4(1):50.
42. Anderle N, Koch A, Gierke B, et al. A platform of patient-derived microtumors identifies individual treatment responses and therapeutic vulnerabilities in ovarian cancer. *Cancers (Basel).* 2022;14(12):2895.
43. Anderle N, Schäfer-Ruoff F, Staebler A, et al. Breast cancer patient-derived microtumors resemble tumor heterogeneity and enable protein-based stratification and functional validation of individualized drug treatment. *J Exp Clin Cancer Res.* 2023;42(1):210.
44. Przystal JM, Becker H, Canjuga D, et al. Targeting CSF1R alone or in combination with PD1 in experimental glioma. *Cancers.* 2021;13(10):2400.
45. Serano RD, Pegram CN, Bigner DD. Tumorigenic cell culture lines from a spontaneous VM/Dk murine astrocytoma (SMA). *Acta Neuropathol.* 1980;51(1):53–64.
46. Koch MS, Czemmel S, Lennartz F, et al. Experimental glioma with high bHLH expression harbor increased replicative stress and are sensitive toward ATR inhibition. *Neurooncol. Adv..* 2020;2(1):vdaa115.
47. Abdelfattah N, Kumar P, Wang C, et al. Single-cell analysis of human glioma and immune cells identifies S100A4 as an immunotherapy target. *Nat Commun.* 2022;13(1):767.
48. Neftel C, Laffy J, Filbin MG, et al. An integrative model of cellular states, plasticity, and genetics for glioblastoma. *Cell.* 2019;178(4):835–849.e21.
49. Reimand J, Kull M, Peterson H, Hansen J, Vilo J. g:profiler—a web-based toolset for functional profiling of gene lists from large-scale experiments. *Nucleic Acids Res.* 2007;35(Web Server issue):W193–W200.
50. Vanasse GJ, Winn RK, Rodov S, et al. Bcl-2 overexpression leads to increases in suppressor of cytokine signaling-3 expression in B cells and de novo follicular lymphoma. *Mol Cancer Res.* 2004;2(11):620–631.
51. Weller M, van den Bent M, Preusser M, et al. EANO guidelines on the diagnosis and treatment of diffuse gliomas of adulthood. *Nat Rev Clin Oncol.* 2021;18(3):170–186.
52. Zeren N, Afzal Z, Morgan S, et al. The chemokine receptor CCR1 mediates microglia stimulated glioma invasion. *Int J Mol Sci .* 2023;24(6):5136.
53. Zhang X, Chen L, Dang W-q, et al. CCL8 secreted by tumor-associated macrophages promotes invasion and stemness of glioblastoma cells via ERK1/2 signaling. *Lab Investig.* 2020;100(4):619–629.
54. Kiyasu Y, Kawada K, Hirai H, et al. Disruption of CCR1-mediated myeloid cell accumulation suppresses colorectal cancer progression in mice. *Cancer Lett.* 2020;487(1):53–62.
55. Masui H, Kawada K, Itatani Y, et al. Synergistic antitumor activity by dual blockade of CCR1 and CXCR2 expressed on myeloid cells within the tumor microenvironment. *Br J Cancer.* 2024;131(1):63–76.
56. Ou DL, Chen CW, Hsu CL, et al. Regorafenib enhances antitumor immunity via inhibition of p38 kinase/Creb1/Klf4 axis in tumor-associated macrophages. *J ImmunoTher Cancer.* 2021;9(3):e001657.

57. Tutusaus A, Stefanovic M, Boix L, et al. Antiapoptotic BCL-2 proteins determine sorafenib/regorafenib resistance and BH3-mimetic efficacy in hepatocellular carcinoma. *Oncotarget*. 2018;9(24):16701–16717.
58. Sofer S, Lamkiewicz K, Armoza Eilat S, et al. A genome-wide CRISPR activation screen reveals Hexokinase 1 as a critical factor in promoting resistance to multi-kinase inhibitors in hepatocellular carcinoma cells. *FASEB J*. 2022;36(3):e22191.
59. Maurer GD, Tritschler I, Adams B, et al. Cilengitide modulates attachment and viability of human glioma cells, but not sensitivity to irradiation or temozolomide in vitro. *Neuro-Oncology*. 2009;11(6):747–756.
60. Wang Z, Zhu Q, Li X, et al. TOP2A inhibition reverses drug resistance of hepatocellular carcinoma to regorafenib. *Am J Cancer Res*. 2022;12(9):4343–4360.
61. Shi W, Zhang S, Ma D, et al. Targeting SphK2 reverses acquired resistance of regorafenib in hepatocellular carcinoma. *Front Oncol*. 2020;10(1).
62. Karabicici M, Azbazdar Y, Ozhan G, et al. Changes in Wnt and TGF-β signaling mediate the development of regorafenib resistance in hepatocellular carcinoma cell line HuH7. *Front Cell Dev Biol*. 2021;9(1):639779.
63. Shigeta K, Matsui A, Kikuchi H, et al. Regorafenib combined with PD1 blockade increases CD8 T-cell infiltration by inducing CXCL10 expression in hepatocellular carcinoma. *J ImmunoTher Cancer*. 2020;8(2):e001435.
64. Mirone G, Perna S, Shukla A, Marfe G. Involvement of Notch-1 in resistance to regorafenib in colon cancer cells. *J Cell Physiol*. 2016;231(5):1097–1105.
65. Song X, Shen L, Tong J, et al. Mcl-1 inhibition overcomes intrinsic and acquired regorafenib resistance in colorectal cancer. *Theranostics*. 2020;10(18):8098–8110.
66. Puris E, Petralla S, Auriola S, et al. Monoacylglycerol lipase inhibitor JJKK048 ameliorates ABCG2 transporter-mediated regorafenib resistance induced by hypoxia in triple negative breast cancer cells. *J Pharm Sci*. 2023;112(9):2581–2590.